Heliyon 7 (2021) e08634

Contents lists available at ScienceDirect

Heliyon

journal homepage: www.cell.com/heliyon

Research article

Major and trace element compositions of basaltic lavas from western margin of central main Ethiopian rift: enriched asthenosphere vs. mantle plume contribution

Daniel Meshesha [a,b], Takele Chekol [a,b,*], Sileshe Negussia [b,1]

[a] Mineral Exploration, Extraction and Processing Center of Excellence, Addis Ababa Science and Technology University, P.O. Box 16417, Addis Ababa, Ethiopia
[b] Department of Geology, College of Applied Sciences, Addis Ababa Science and Technology University, P.O. Box 16417, Addis Ababa, Ethiopia

ARTICLE INFO

Keywords:
Main Ethiopian rift
Plume
Crustal contamination
Mantle source
Alkaline basalts
Tholeiite basalts

ABSTRACT

Major and trace element data are presented for basaltic lavas from western rift margin of central Main Ethiopian Rift located at Kella area to investigate the processes involved in the petrogenesis of the erupted magmas and the nature of mantle source compositions. Kella area is composed of Quaternary (<1.6 Ma), Miocene (10.6–8.3 Ma) and Oligocene basalts (30-29 Ma) ranging from alkaline to tholeiitic in composition. The geochemical variations of basaltic samples from Kella area exhibit two compositionally distinct basaltic groups. The Oligocene tholeiitic basalts display low MgO (5.29–6.11 wt.%), TiO_2 (2.15–2.47 wt.%), P_2O_5 (0.28–0.34 wt.%), and high ratio of CaO/Al_2O_3 (0.68–0.72) and La/Nb (0.89–1.10). Whereas Quaternary and Miocene alkaline basalts display high MgO (7.40–8.86 wt.%), TiO_2 (2.4–2.53 wt.%), P_2O_5 (0.44–0.52 wt.%) and low ratio of CaO/Al_2O_3 (0.62–0.66) and La/Nb (0.71–0.76). The contrasting incompatible element ratios (e.g., K/Nb, La/Nb, Rb/Zr and Zr/Nb) between tholeiite and alkaline basalts reflect differences in their mantle sources. Major and trace element variations, therefore, reflect the involvement of two geochemically distinct mantle sources in the petrogenesis of Kella basaltic lavas: i) the Oligocene tholeiite basaltic melts derived from enriched asthenosphere mantle source (E-MORB) and ii) the Miocene and Quaternary alkali basaltic melts show a close similarity with ocean island basalts (OIBs) geochemistry, and this end member ascribed to the arrival of Afar plume head. The geochemical modeling reveals that the Oligocene tholeiite basaltic melts produced by an equilibrium melting with 3–5 % degree of partial melting in spinel lherzolite mantle source, whereas the alkali basalts were produced with ~2% degree of partial melting within spinel-garnet lherzolite transition zone mantle sources.

1. Introduction

The East African Rift System (EARS) is several kilometer long currently active intercontinental rifts extending about 2000 km long from the Red Sea/Gulf of Aden in the north to Malawi in the south with widely distributed mafic and felsic volcanic rocks (e.g., Kieffer et al., 2004; Wolfenden et al., 2004; Chorowicz, 2005; Saemundsson, 2010; Ring, 2014; Scoon, 2018). The distribution of magmatism and associated uplifting throughout the EARS is attributed to compositionally distinct Kenya (~45 Ma) and Afar (~30 Ma) plumes (George et al., 1998; Rogers et al., 2000; George and Rogers, 2002; Meshesha and Shinjo, 2008). The Kenya and Afar plumes are believed to be branched from huge, complex and compositionally heterogenous African Superplume beneath southern Africa (Kieffer et al., 2004: Furman, 2007; Meshesha and Shinjo, 2008). As shown in Figure 1a, the EARS includes Ethiopian rift, Kenyan Rift, Afar Depression and the surrounding plateaus.

Whole rock geochemical and isotopic studies in the Ethiopian continental flood basalts and the magmatism in Main Ethiopian Rift show the involvement of compositionally heterogenous Afar mantle plume, asthenospheric mantle and lithospheric mantle in their generation (e.g., Hart et al., 1989; Marty et al., 1996; Stewart and Rogers, 1996; Pik et al., 1998, 1999; Kieffer et al., 2004; Meshesha and Shinjo, 2007, 2008: Beccaluva et al., 2009, 2011; Natali et al., 2016).

The contributions from distinct mantle end-member components [intrinsic Depleted Mantle (DM), Enriched Mantle (EM I & II), High-μ (HIMU) and Primitive Mantle (PREMA)] in different proportions and

* Corresponding author.
E-mail address: takele.chekol@aastu.edu.et (T. Chekol).
[1] Present address: Geology Department, College of Natural and Computational Science, Assosa, Ethiopia.

https://doi.org/10.1016/j.heliyon.2021.e08634
Received 22 July 2021; Received in revised form 22 October 2021; Accepted 15 December 2021

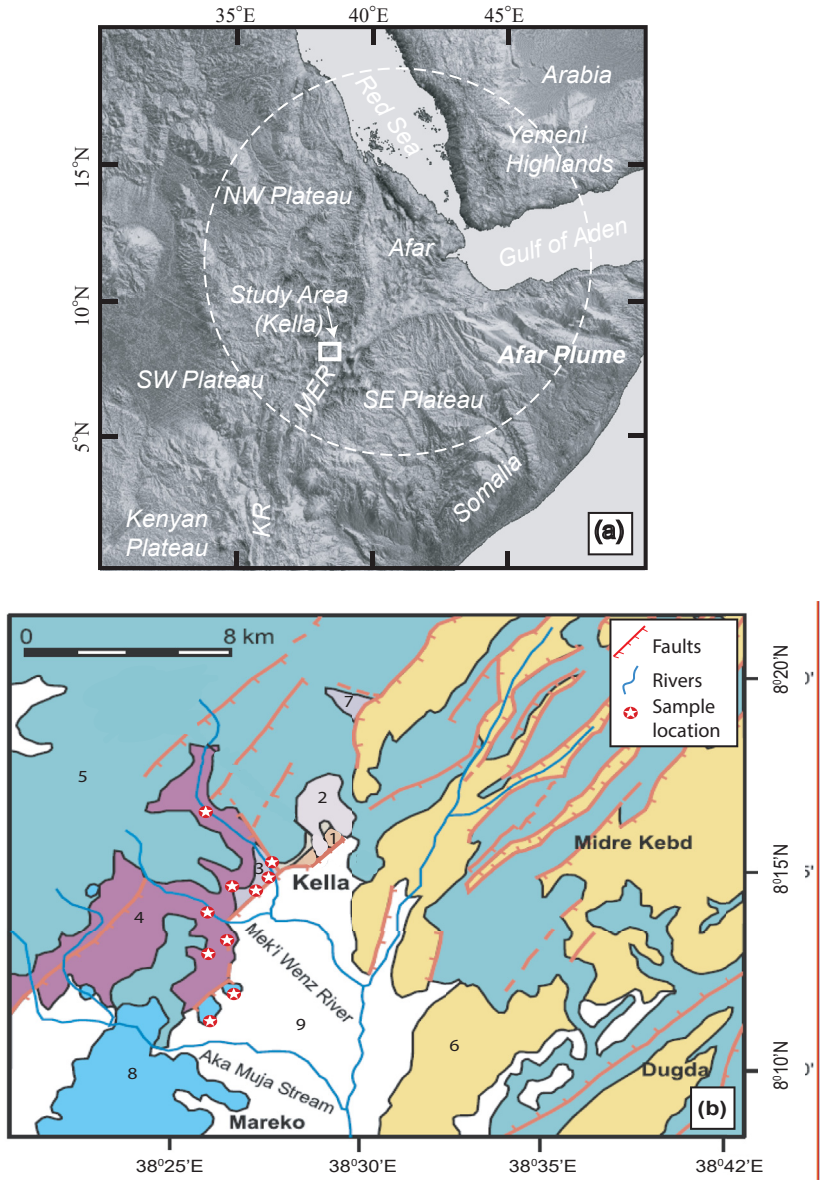

Figure 1. Location of Kella area a) Map of northeastern Africa and Arabia (NASA SRTM30) b) Simplified geological map of Kella area; (1) Kella metamorphic rocks, (2) Mesozoic cover, (3) Oligocene plateau volcanics (32-29 Ma), (4) Miocene plateau volcanics (Guraghe Basalts: 10.6–8.3 Ma), (5) Miocene-Pliocene rift-shoulder trachytic-rhyolitic volcanics (<5 Ma) and pyroclastic deposits (5.2–2.6 Ma), (6) Pyroclastic deposits (2.54–1.7 Ma), (7) Quaternary lava flow (<1.6 Ma), (8) Wonji Basalts (<1.6 Ma), (9) Lacustrine sediments. Dashed circle indicating the extent of Afar Plume.

their interaction with subcontinental lithospheric and asthenosphere mantle for the genesis of magmas in the EARS have been suggested by many authors (Stewart and Rogers, 1996; Pik et al., 1998, 1999; Kieffer et al., 2004: Meshesha and Shinjo, 2007, 2008; Beccaluva et al., 2009, 2011; Feyissa et al., 2017). Nonetheless, the involvement of lithospheric component having high $^{87}Sr/^{86}Sr_i$, and elevated $^{207}Pb/^{204}Pb_i$ and $^{208}Pb/^{204}Pb_i$ for a given $^{206}Pb/^{204}Pb_i$ (Pik et al., 1998, 1999; Shinjo et al., 2011; Feyissa et al., 2017) and/or continental crustal material characterized by higher incompatible trace element ratios (e.g., Ba/Nb and Rb/Nb), $^{87}Sr/^{86}Sr$ and non-radiogenic Pb isotopes (Baker et al., 2000; Meshesha and Shinjo, 2007, 2010) is still disputed.

In order to investigate the involvements of variable mantle sources in the genesis of basalts the Kella area (western rift wall, Figure 1b) is of a great interest because it represents both pre- and post-rift basaltic rocks; the plateau (Oligocene flood basalt; 30-29 Ma), the rift escarpment (Miocene basalt; 10.6–8.3 Ma) and the rift floor (Quaternary basalt; <1.6 Ma). Though there are many previous studies on the geology and geochemistry of volcanic rocks in various parts of the Ethiopian Plateau (Berhe et al., 1987; Hofmann et al., 1997; Pik et al., 1998, 1999; Ukstins et al., 2002; Kieffer et al., 2004; Meshesha and Shinjo, 2007; Beccaluva et al., 2009) and Main Ethiopian Rift (MER; Moore and Davidson, 1978; WoldeGabriel et al., 1990; Chernet et al., 1998; Ayalew, 2000; Wolfenden et al., 2004; Ayalew et al., 2016), there are no geochemical data for Kella area that situated at the western rift margin of Central Main Ethiopian Rift (Figure 1a) except geochronological data (Abebe et al., 2010 and references therein).

In this paper we present new data including petrographic, major and trace-element data for basaltic rocks from the plateau, the rift escarpment and the rift floor of Kella area, western rift margin of Central Main Ethiopian Rift (Figure 1b). Therefore, our new petrographic, major and trace-element data can be used to constrain the processes involved in the compositional variations of Kella basaltic lavas and their mantle source components during transition from Oligocene, Miocene to Quaternary magmatism.

2. Geological setting

Ethiopian magmatism was started between 45-35 Ma in southern Ethiopia but it is smaller in volume and spatial distribution than the succeeding Oligocene continental flood basalts that were erupted between 31 and 28 Ma (Davidson and Rex, 1980; Berhe et al., 1987; Ebinger et al., 1993; George et al., 1998). The volumetrically huge

amount (greater than 350,000 km^3) of Oligocene continental flood basalts were erupted within short period of time (Hofmann et al., 1997; Pik et al., 1998; Ukstins et al., 2002; Meshesha and Shinjo, 2007; Beccaluva et al., 2009) and forming about 2000 m thick volcanic succession at northwestern, southwestern and southeastern Ethiopian Plateaus (Figure 1a). The Oligocene continental flood basalts were linked and coincided with the arrival of the Afar mantle plume head (Mohr and Zanettin, 1988; Hofmann et al., 1997; Pik et al., 1998, 1999; Ayalew et al., 2002; Kieffer et al., 2004; Meshesha and Shinjo, 2008; Beccaluva et al., 2009; Natali et al., 2016) at the initial stage of lithospheric extension (e.g., Mohr, 1983; Berhe et al., 1987). The continental flood basalt of northwestern Ethiopian Plateau spatially subdivided by their contrasting compositions as low-Ti (LT-type) basalt and high-Ti (HT1-and HT2-type) basalt (Pik et al., 1998, 1999; Beccaluva et al., 2009). The LT and HT1 are tholeiitic while the HT2 are transitional in compositions (Beccaluva et al., 2009; Natali et al., 2016).

In the Ethiopian Plateau, the Oligocene magmatic activity is ended with the build-up of alkaline central type shield volcanism, for example, 23 Ma Choke and Guguftu (Kieffer et al., 2004) and 11.2–7.8 Ma Wollega shield volcano (Berhe et al., 1987) in the northwestern plateau. Compositionally, the shield volcanoes are bimodal.

Recent magmatic activities were mainly concentrated in the Main Ethiopian Rift (MER) that bisecting the Ethiopian Plateau into northwestern and southeastern sectors. The magmatism in MER is characterized by temporally and spatially variable fissural and central basalts and started in the early Miocene (20–21 Ma; WoldeGabriel et al., 1990; Ebinger et al., 1993; Stewart and Rogers, 1996; George et al., 1998; George and Rogers, 2002; Bonini et al., 2005; Furman, 2007). These episodic magmatisms (Girdler, 1983; WoldeGabriel et al., 1990) were distributed into structurally distinct Northern (NMER; 11-10 Ma), Central (CMER; 5-3 Ma) and Southern (SMER; 18-15 Ma) segments of MER (Hart et al., 1989; WoldeGabriel et al., 1990; Hayward and Ebinger., 1996; Chernet et al., 1998; Wolfenden et al., 2004; Bonini et al., 2005; Corti, 2009). The volcanic rocks in the MER are bimodal in nature (basalt-rhyolite) with clear absence of intermediate rocks (Ayalew, 2000). The rift volcanic rocks are transitional to alkaline in composition and show peralkaline character for the more evolved volcanic rocks (Peccerillo et al., 1995; Trua et al., 1999; Ayalew, 2000).

Kella, the study area, at the western rift margin of Central Main Ethiopian Rift is covered by patches of Precambrian metamorphic rocks and Mesozoic sedimentary rocks (Abebe et al., 2010 and this study) at the base of the rift escarpment, near the village of Kella. However, the larger portion of the Kella area is covered by Tertiary-Quaternary volcanic rocks and recent sediments (Figure 1b). The volcanic rocks in the study area are bimodal in composition, which comprises of basalt, rhyolite and ignimbrite, where the basalts occur only in the southwestern part of Kella area (Figure 1b). The basalts in Kella area are overlain by Miocene-Pliocene rift-shoulder trachytic-rhyolitic volcanic (<5 Ma) and pyroclastic deposits (5.2–2.6 Ma). The basalts include Oligocene (30-29 Ma), Miocene (10.6–8.3 Ma) and Quaternary (<1.6 Ma) age (Abebe et al., 2010). The Oligocene (30-29 Ma) basalts are aphanitic in texture and cover an area of 4.3 km^2 with an exposed thickness of 2000 m. Both Miocene (10.6–8.3

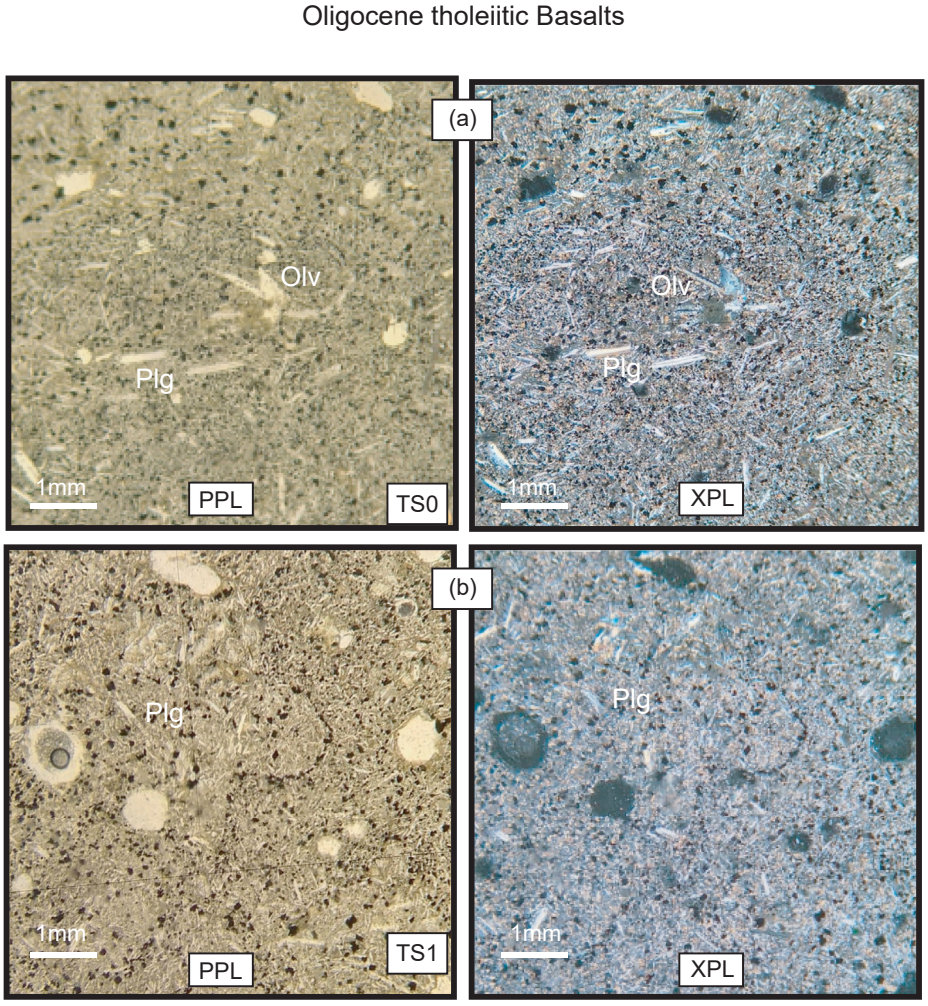

Figure 2. Selected representative photomicrographs of Oligocene basalts in the Kella area. In Plane Polarized Light (PPL) and Cross-polarize (XPL). Both a) and b) are aphyric in texture.

Ma) and Quaternary (<1.6 Ma) basalts are aphyric to porphyritic in texture and cover about an area of 16 km^2 southwest of Kella. The Miocene (10.6–8.3 Ma) basalts are dominantly cover the rift shoulder in the southwestern part of the area while the Quaternary basalts found south of Kella village in the rift floor and are generally affected by northeast trending faults.

3. Petrography of basaltic rocks from Kella area

On the basis of petrological characteristics samples from the Oligocene which is part of the continental flood basalts are tholeiitic basalts, whereas the Miocene and Quaternary are alkali basalts.

Representative photomicrographs from the Oligocene tholeiitic, Miocene and Quaternary alkali basalts are shown in Figures 2 and 3. The Oligocene tholeiitic basalts are holocrystalline and aphyric in texture with less than 1% micro phenocrysts (dominate plagioclase and minor olivine). The groundmass minerals are plagioclase, olivine, clinopyroxene and opaque crystals in variable proportions.

The Miocene alkali basalts are characterized by holocrystalline and moderately phyric texture with phenocrysts up to 10%. Phenocryst minerals are 1–1.5 mm subhedral clinopyroxene (5%), 0.5–1.5 mm olivine (4%) and < 1 mm plagioclase (1%) set in groundmasses containing plagioclase, clinopyroxene, olivine and opaque minerals.

The Quaternary alkali basalts are moderately phyric in texture. Phenocrysts reach up to ~5%. Similar to the other groups they are holocrystalline. This group of basalts has phenocryst assemblages of 0.5–1 mm olivine (2 %) and 1–2 mm clinopyroxene (2 %) and < 1 mm plagioclase (<1%). Olivine and clinopyroxene occur as subhedral

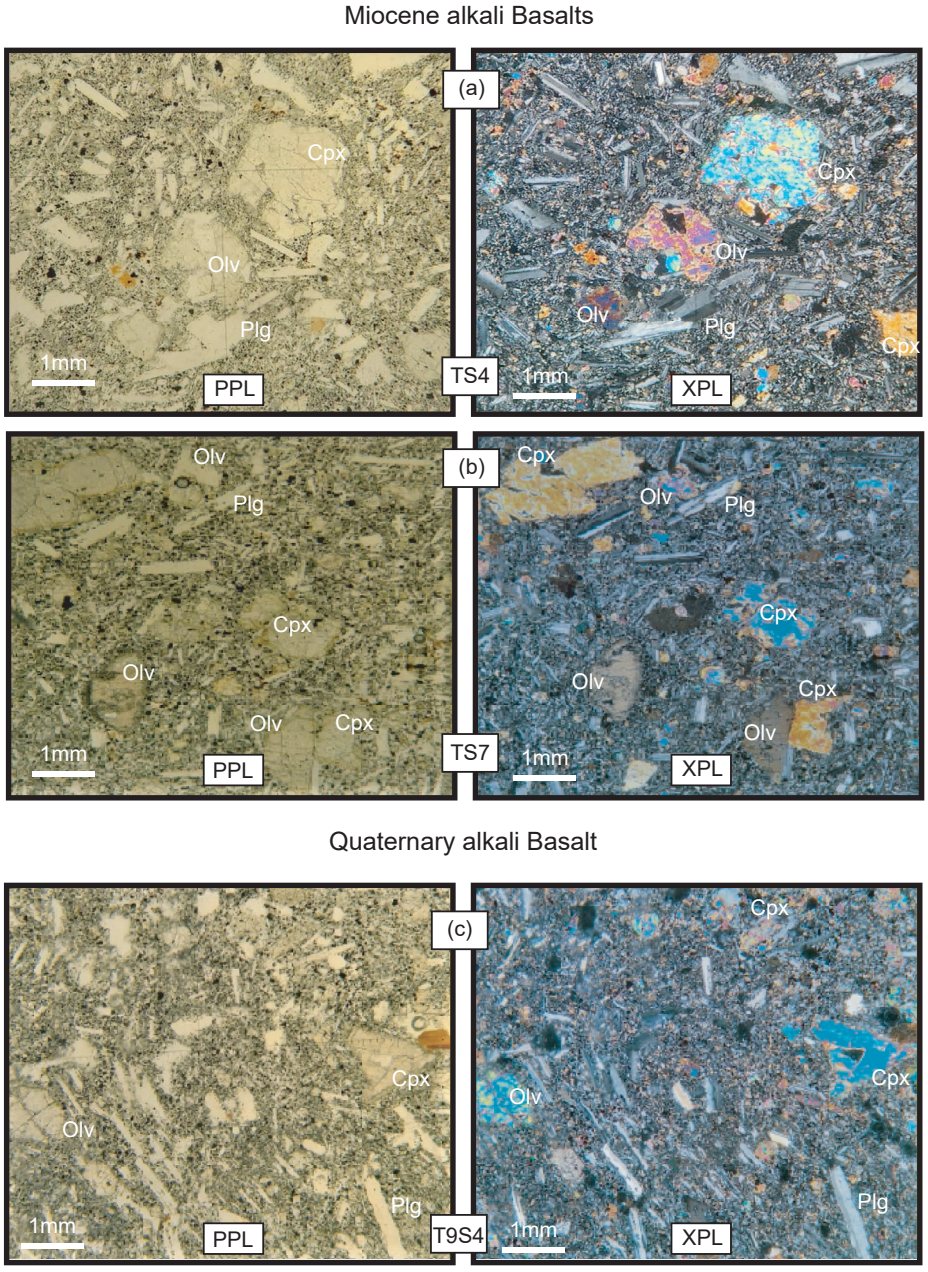

Figure 3. Selected representative photomicrographs of Miocene (a and b) and Quaternary (c) alkali basalts in the Kella area. In Plane Polarized Light (PPL) and Cross-polarize (XPL).

crystals. The groundmass is composed of microcrystalline plagioclase, clinopyroxene, olivine, and opaque minerals in variable proportions. The groundmass is characterized by intergranular texture.

4. Analytical method

Eleven representative fresh samples were selected for major and trace element analysis (Tables 1 and 2). Samples were prepared for whole-rock geochemical analysis in Australia Laboratory Services (ALS) at Addis Ababa, Ethiopia. The preparation was started by removing the altered part and drying the samples in drying ovens at 100̊c. Then, the dried samples were crushed to coarse chips from which fresh chips were carefully hand-picked or split using a rotary splitter. The hand-picked chips were pulverized into 75 microns and then the powder was packed and sent to Australian Laboratory Services (ALS), Ireland.

The whole-rock major elements reported as major elements SiO_2, Al_2O_3, Fe_2O_3, MgO, CaO, Na_2O, K_2O, TiO_2, MnO and P_2O_5 were determined on the lithium metaborate (sample: flux ratio is 1:5) fused glass beads by using X-ray fluorescence spectrometry (S4 PIONEER XRF) at ALS, Ireland.

To determine the concentration of trace elements including rare earth elements (REE), the mixture of powder sample and lithium metaborate flux (sample: flux ratio is 1:5) was fused in a furnace at 1000 °C. The resulting melt is then cooled and dissolved in 100 mL of 4% HNO_3/2% HCl solution. Then the solutions were analyzed for trace elements Rb, Ba, Sc, V, Cr, Co, Ni, Sr, Y, Zr, Nb, Cs, Hf, Ta, Pb, Th, U, La, Ce, Pr, Nd, Sm, Eu, Gd, Tb, Dy, Ho, Er, Tm, Yb and Lu by Inductively Coupled Plasma Mass Spectrometry (ICP-MS, Agilent 7700 technology).

Reproducibility and repeatability of the data were checked using blank and international rock standard [South Africa Reference Material (SARM-5; https://www.mintek.co.za/technical-divisions/analytical-services-asd/sarm/sarm-certificates) and Ore Research & Exploration Analytical Solution (OREAS-122; https://www.oreas.com/crm/oreas-122)].

5. Whole-rock compositions

5.1. Major elements

Major element data for Kella volcanic rocks are reported in Table 1. The MgO contents for Oligocene basalts are ranging from 5.29-6.11 wt. %, for Miocene and Quaternary basalts are between 8.21-8.86 and 7.4–8.45 wt. %, respectively. Relatively Miocene basalts are more magnesium rich than the Oligocene and Quaternary basalts. In the total Alkali-Silica (TAS) classification diagram of Le Bas et al. (1986), all Kella samples are basalts in composition and subdivided into alkaline and tholeiite series (Figure 4a). As shown in Figure 4, Oligocene basalts are tholeiite series and plot with Low-Ti basalts of Pik et al. (1998, 1999) while the Miocene and Quaternary basalts are alkaline series and plot with High-Ti basalts (Pik et al., 1998, 1999) and NMER western rift wall basalts (Ayalew et al., 2018). The variations of Kella basaltic lavas are clearly demonstrated in their CIPW normative (Table 1 and Figure 4b). The Oligocene tholeiitic basalts are quartz normative whereas Miocene and Quaternary alkali basalts are olivine and nepheline normative.

Selected major element versus MgO (wt. %) plots are shown in Figure 5. In most plots, the Kella basaltic rocks show two distinct trends: 1) for the Miocene and Quaternary alkali basalts and 2) for the Oligocene tholeiitic basalts. In all groups, TiO_2, Na_2O, K_2O and P_2O_5, show negative correlations with MgO (Figure 5c, e, g and h). Al_2O_3 is positively correlated with MgO in the Oligocene tholeiite basalts and negatively

Table 1. Major (wt. %, totals as wet conditions) and CIPW normative for basaltic lavas from the Kella area.

Type	Oligocene flood basalt		Lower Miocene basalt					Quaternary basalt			Standard	
Sample	TS0	TS1	TS4	TS7	TS9	TS11	T9S9	T9S2	T9S3	T9S4	SY-4	SARM-5
Lat. (°)	38.28	38.28	38.28	38.26	38.28	38.26	38.27	38.27	38.27	38.28		
Lon. (°)	8.15	8.15	8.14	8.14	8.16	8.12	8.14	8.11	8.14	8.11		
Elev. (m)	1990	1980	2020	2180	2210	2230	2001	1916	1925	1927		
SiO_2 (wt %)	50.20	51.20	47.15	47.84	47.57	47.43	47.59	47.76	46.84	47.14	49.60	50.55
Al_2O_3	14.58	13.88	15.35	15.42	15.46	15.38	15.60	15.52	15.58	15.24	20.56	4.11
Fe_2O_3	11.88	13.19	11.87	12.08	11.97	11.88	12.12	12.12	11.94	11.95	6.19	12.62
MgO	6.11	5.29	8.21	8.58	8.86	8.37	8.36	7.59	7.4	8.45	0.52	25.2
CaO	10.50	9.56	9.80	10.00	10.30	9.83	9.79	10.10	9.83	9.86	7.94	2.58
Na_2O	2.83	3.04	3.13	3.10	2.91	3.15	3.11	3.15	3.11	3.10	7.12	0.34
K_2O	0.36	0.71	1.06	1.03	0.85	1.05	1.06	1.06	1.08	1.02	1.66	0.08
TiO_2	2.15	2.47	2.47	2.50	2.40	2.50	2.51	2.53	2.51	2.48	0.28	0.18
MnO	0.18	0.18	0.17	0.18	0.18	0.17	0.18	0.18	0.18	0.18	0.11	0.22
P_2O_5	0.28	0.34	0.51	0.50	0.44	0.51	0.51	0.52	0.51	0.50	0.13	0.01
LOI	0.40	0.36	-0.36	-0.26	-0.37	-0.48	-0.43	0.20	0.51	-0.35		
Total	99.69	100.50	99.66	101.30	100.90	100.10	100.70	101.05	100.00	99.88	94.11	95.89
CIPW normative												
Qt	6.78	8.37										
Or	2.13	4.20	6.26	6.09	5.02	6.21	6.26	6.26	6.38	6.03		
Ab	23.95	25.72	26.49	26.23	24.62	26.65	26.32	26.65	26.32	26.23		
An	26.02	22.13	24.70	25.12	26.61	24.73	25.48	25.08	25.36	24.66		
Di	13.59	11.82	9.84	10.29	10.87	9.86	9.13	10.53	9.37	10.17		
Hy	8.92	7.70	7.64	8.72	10.41	7.78	8.94	9.22	8.39	7.73		
Ol			5.78	5.52	4.64	5.95	5.37	3.37	3.99	6.03		
Il	0.39	0.39	0.36	0.39	0.39	0.36	0.39	0.39	0.39	0.39		
Hm	11.88	13.19	11.87	12.08	11.97	11.88	12.12	12.12	11.94	11.95		
Ti	4.78	5.57	5.59	5.64	5.39	5.67	5.66	5.71	5.66	5.59		
Ap	0.66	0.81	1.21	1.18	1.04	1.21	1.21	1.23	1.21	1.18		
Total	99.09	99.88	99.75	101.26	100.97	100.30	100.86	100.56	99.01	99.95		

Table 2. Trace element data (ppm) for basaltic lavas from the Kella area.

Type	Oligocene flood basalt			Lower Miocene basalt					Quaternary basalt			Standard		% error
Sample	TS0	TS1	TS2	TS4	TS7	TS9	TS11	T9S9	T9S2	T9S3	T9S4	REE-1	OREAS-122	
Lat. (°)	38.28	38.28	38.28	38.28	38.26	38.28	38.26	38.27	38.27	38.27	38.28			
Lon. (°)	8.15	8.15	8.15	8.14	8.14	8.16	8.12	8.14	8.11	8.14	8.11			
Elev. (m)	1990.00	1980.00	2000	2020.00	2180.00	2210.00	2230.00	2001.00	1916.00	1925.00	1927.00			
Sc	35.00	33.00	34.5	25.00	24.00	25.00	24.00	27.00	26.00	25.00	24.00			
V	362.00	415.00	389	300.00	304.00	309.00	294.00	327.00	300.00	307.00	318.00	10.00	29.00	0.15
Cr	100.00	50.00	75.5	360.00	330.00	460.00	310.00	360.00	330.00	320.00	340.00	310.00	50.00	
Co	42.00	41.00	42	42.00	43.00	45.00	41.00	49.00	44.00	44.00	47.00			
Ni	42.00	6.00	24.5	111.00	108.00	118.00	106.00	122.00	120.00	101.00	114.00			
Rb	5.80	10.70	8.7	19.10	18.60	12.60	18.50	19.60	18.30	19.40	18.70	1025.00	83.70	
Sr	378.00	385.00	382	667.00	672.00	636.00	658.00	691.00	684.00	726.00	698.00	124.50	137.50	0.02
Y	31.00	34.80	33.4	20.80	20.70	21.10	19.80	21.60	20.90	21.80	21.10	5530.00	13.50	0.04
Zr	160.00	211.00	186	142.00	139.00	113.00	131.00	141.00	140.00	147.00	142.00	>10000	276.00	
Nb	15.10	24.60	20.3	33.00	32.00	29.00	32.80	33.30	32.60	35.20	33.10	>2500	10.30	0.23
Cs	0.15	0.18	0.16	0.16	0.17	0.15	0.17	0.20	0.17	0.13	0.13	1.04	0.68	0.07
Ba	201.00	241.00	221.5	348.00	345.00	312.00	340.00	352.00	341.00	392.00	340.00	99.40	974.00	0.00
La	16.70	22.00	4.8	24.90	24.20	21.20	23.50	25.20	24.40	27.10	24.70	1620.00	20.80	0.01
Ce	34.90	50.40	1.3	52.90	50.50	44.60	50.80	52.60	52.30	55.00	53.00	3990.00	45.80	0.00
Pr	5.06	6.63	1.79	6.54	6.32	5.72	6.38	6.61	6.43	6.77	6.54	430.00	5.12	0.01
Nd	22.90	28.80	0.55	27.60	26.60	24.20	26.70	27.40	27.40	27.40	27.30	1410.00	20.00	0.03
Sm	5.73	6.66	19.8	5.93	5.46	5.12	5.70	5.64	5.79	5.88	5.90	374.00	3.68	0.01
Eu	1.93	2.08	43.1	1.88	1.90	1.89	1.86	1.95	1.99	1.88	1.95	23.60	1.03	0.01
Gd	6.55	7.06	6.34	5.45	5.16	5.52	5.16	5.21	5.30	5.51	5.44	428.00	3.15	0.01
Tb	0.96	1.02	26.3	0.76	0.71	0.76	0.71	0.75	0.75	0.73	0.73	103.50	0.45	0.03
Dy	6.22	6.78	6.3	4.46	4.34	4.57	4.37	4.56	4.48	4.35	4.23	850.00	2.74	0.07
Ho	1.19	1.27	2.00	0.79	0.81	0.80	0.76	0.83	0.83	0.80	0.80	202.00	0.52	0.03
Er	3.23	3.40	6.80	2.10	2.06	2.18	2.09	2.19	2.25	2.02	1.96	670.00	1.40	0.01
Tm	0.46	0.51	1.00	0.29	0.28	0.31	0.29	0.29	0.30	0.32	0.30	107.50	0.21	0.04
Yb	2.96	3.22	6.52	1.95	1.82	2.04	1.81	1.89	1.86	1.99	1.83	680.00	1.48	0.04
Lu	0.44	0.45	1.23	0.27	0.26	0.29	0.25	0.30	0.27	0.27	0.27	91.50	0.23	0.06
Hf	3.70	5.00	3.3	3.10	3.10	2.70	3.20	3.10	3.30	3.40	3.20	478.00	6.60	0.08
Ta	1.10	1.50	0.48	1.70	1.80	2.50	3.50	1.60	1.60	1.80	1.50	238.00	4.20	4.69
Th	1.42	2.16	3.09	2.46	2.27	2.07	2.23	2.42	2.44	2.38	2.30	720.00	5.33	0.03
U	0.34	0.65	0.42	0.63	0.62	0.44	0.62	0.57	0.63	0.65	0.61	137.50	384.00	

correlated in the Miocene and Quaternary alkali basalts (Figure 5f). CaO shows positive trends for the Oligocene tholeiitic basalts, as well as the Miocene and the Quaternary alkali basalts (Figure 5b). Fe_2O_3 is almost constant in Miocene and Quaternary alkali basalts with MgO >6.11 wt. %, but in the Oligocene tholeiitic basalts Fe_2O_3 is negatively correlated with MgO (Figure 5d).

5.2. Trace elements

Trace element data of the Kella basaltic rocks are shown in Table 2. The compatible element Ni is positively correlated with MgO in all groups (Figure 6g). Almost constant Y with increasing MgO contents are observed in the Miocene and Quaternary alkali basalts, while negative correlation is observed for Oligocene tholeiite (Figure 6d). V show slight positive correlations with MgO for the Miocene and Quaternary alkali basalts, while negatively correlated in Oligocene tholeiite basalts (Figure 6f). Nb, Zr, Rb, Ba and Sr versus MgO show negative correlation in all basaltic groups (Figure 6a, b, c, d and h). In the plots of Nb, Rb, Ba and Sr (Figure 6a, c, e and f) two distinct negative trends one representing the Miocene and Quaternary alkali basalts and the other one representing the Oligocene tholeiitic basalts are observed.

The primitive mantle-normalized multi-element patterns are shown in Figures 7a, c and e. The general patterns in all groups show a close similarity to oceanic island basalts (OIB-type) than that of a typical normal mid-oceanic basalt (N-MORB) (Sun and McDonough, 1989). Even though all groups show a general OIB pattern, there are some different features between the Oligocene tholeiitic basalts and the other groups. The Miocene and Quaternary alkali basalts plotted closer to OIB pattern but the Oligocene tholeiitic basalts are relatively lower than the average OIB. Moreover, the Miocene and Quaternary Alkali groups show slight enrichment in HFSE (Nb and Ta) compared to the LREE (La and Ce), and LILE (except Ba) which is a typical characteristic feature in Oceanic Island basalts (OIB) patterns (Weaver, 1991). In the other hand, HFSE (Nb and Ta) in the Oligocene tholeiitic basalts show no significant enrichment relative to LREE (La and Ce) and LILE. In general, the Miocene and Quaternary Alkali basaltic groups are characterized by relatively higher HFSE/LREE and HFSE/LILE ratios compared with the Oligocene tholeiitic group (Figure 7). The Miocene and Quaternary alkali basalts are characterized by slight positive anomalies of Ba than the Oligocene tholeiitic basalts.

Chondrite-normalized rare earth element (REE) patterns are given in Figures 7b, d and f. The rare earth element patterns of alkaline basalts show enrichment of light rare earth element (LREE) relative to heavy rare earth elements (HREE) analogues to typical ocean island basalt (OIB) like pattern (Sun and McDonough, 1989). The tholeiite basalts show slight enrichment in heavy rare earth elements (HREE) than the alkaline basalts (Figure 7b). The MREE to HREE patterns of Oligocene tholeiitic basalts are analogues to typical Mid Oceanic basalt (MORB) like pattern (Sun and McDonough, 1989) (Figure 7b). The Oligocene tholeiitic basalts have lower ratios of LREE/HREE ($(La/Yb)_N$ = 4.04–4.90), LREE/MREE

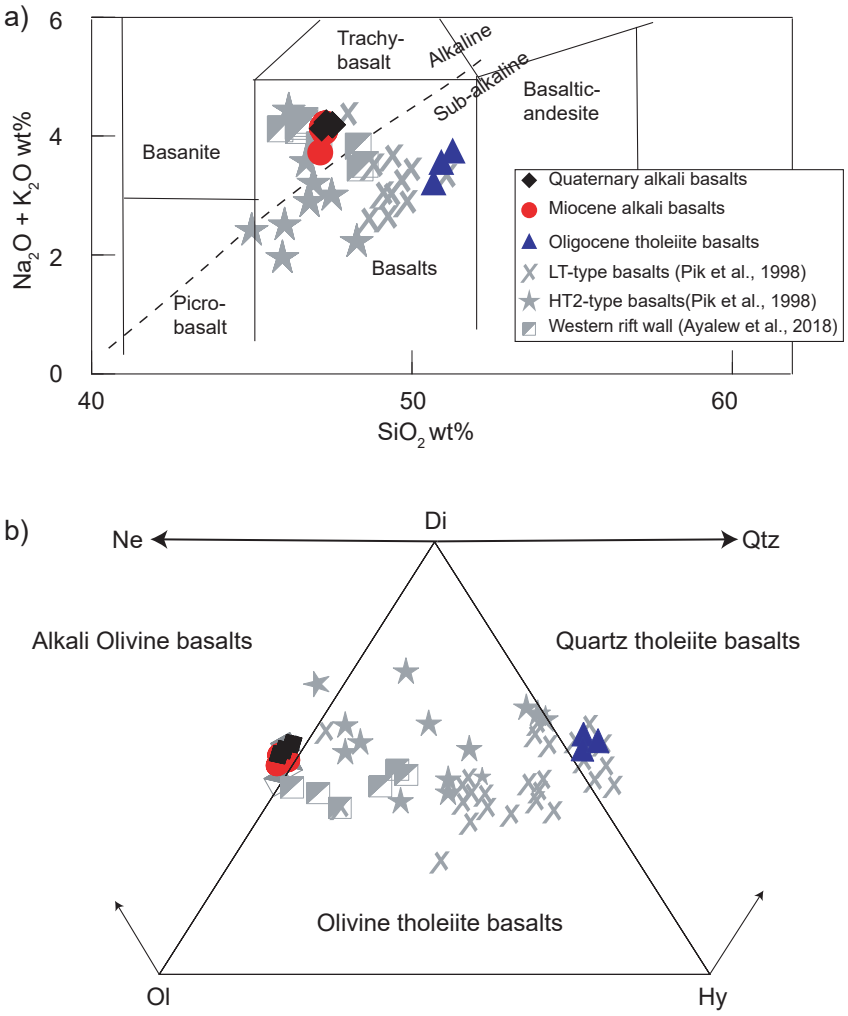

Figure 4. a) Total alkali-silica ($Na_2O + K_2O$) versus SiO_2 diagram (Le Bas et al., 1986) and b) CIPW-normative compositions diagram (Thompson et al., 1983) of the Kella basaltic rocks. LT- and HT2-type basalts are from Pik et al. (1998, 1999) and NMER western rift wall basalts are from Ayalew et al. (2018). The dividing line of alkaline-sub alkaline is from Irvine and Baragar (1971). Ne=Nepheline, Hy = Hypersthene, Di = Diopside, Ol = Olivine and Qtz = Quartz.

$((La/Sm)_N$ = 1.88–2.13) and MREE/HREE ($(Tb/Yb)_N$ = 1.44–1.47, $(Dy/Yb)_N$ = 1.40–1.41) as compared to the other two groups. The Miocene and Quaternary alkali basalts, in the other hand, show higher ratios of LREE/HREE ($(La/Yb)_N$ = 7.45–9.56 and 9.40–9.76, respectively), LREE/MREE ($(La/Sm)_N$ = 2.66–2.88 and 2.70–2.97, respectively) and MREE/HREE ($(Tb/Yb)_N$ = 1.70–1.80 and 1.66–1.81; $(Dy/Yb)_N$ = 1.45–1.61 and 1.46–1.61, respectively) relative to the tholeiitic basalts (Figure 7).

6. Discussion

The geochemical data presented for basaltic samples from Kella area exhibit two compositionally distinct basaltic groups; 1) tholeiitic [Oligocene basalts (30-29 Ma)] and 2) alkali basalts [Miocene (10.6–8.3 Ma); Quaternary (<1.6 Ma)]. The compositional variations between the two groups may indicate either different magmatic processes (partial melting, fractional crystallization and crustal contamination) or variable contributions of mantle source (asthenosphere, mantle plume and sub-continental lithospheric mantle) in their petrogenesis. Since these basaltic groups have major time gap from each other, it is unlikely that different magmatic processes from a co-magmatic melt could be accountable for the observed compositional variations among the Oligocene, Miocene and Quaternary basalts. Therefore, two possibilities could be responsible for the observed compositional variations that observed among the groups: i) even though these basaltic groups cannot be co-magmatic, they might share similar mantle source that melted in different periods and the compositional variations might be due to magmatic processes like partial melting, fractional crystallization and crustal contamination and ii) the compositional variations could be due to differences in their mantle sources. Therefore, below we examine the magmatic processes or the source mantle that contributing for the geochemical variation between tholeiite and alkaline basalts that erupted during the Oligocene, Miocene and Quaternary periods.

6.1. Role of fractional crystallization

The major and trace element variation diagrams show two distinct trends; one for Miocene and Quaternary alkali basalts and the other for the Oligocene tholeiite basalts (Figures 5 and 6). Al_2O_3 versus MgO shows a positive trend in the Oligocene tholeiite basalts, possibly indicating fractionation of plagioclase and olivine, which is a typical fractionation feature in the tholeiitic magmatic series. Petrographic study (Section 3, Figure 2) also support that the Oligocene tholeiitic basalts are with less than 1 % micro phenocrysts (dominate plagioclase and minor olivine). Al_2O_3 versus MgO in the Miocene and Quaternary alkali groups show negative trend indicating that no plagioclase fractionations in these groups. In the plot of CaO versus MgO (Figure 5) the decreasing of CaO with decreasing MgO in the Miocene and Quaternary alkali basalts

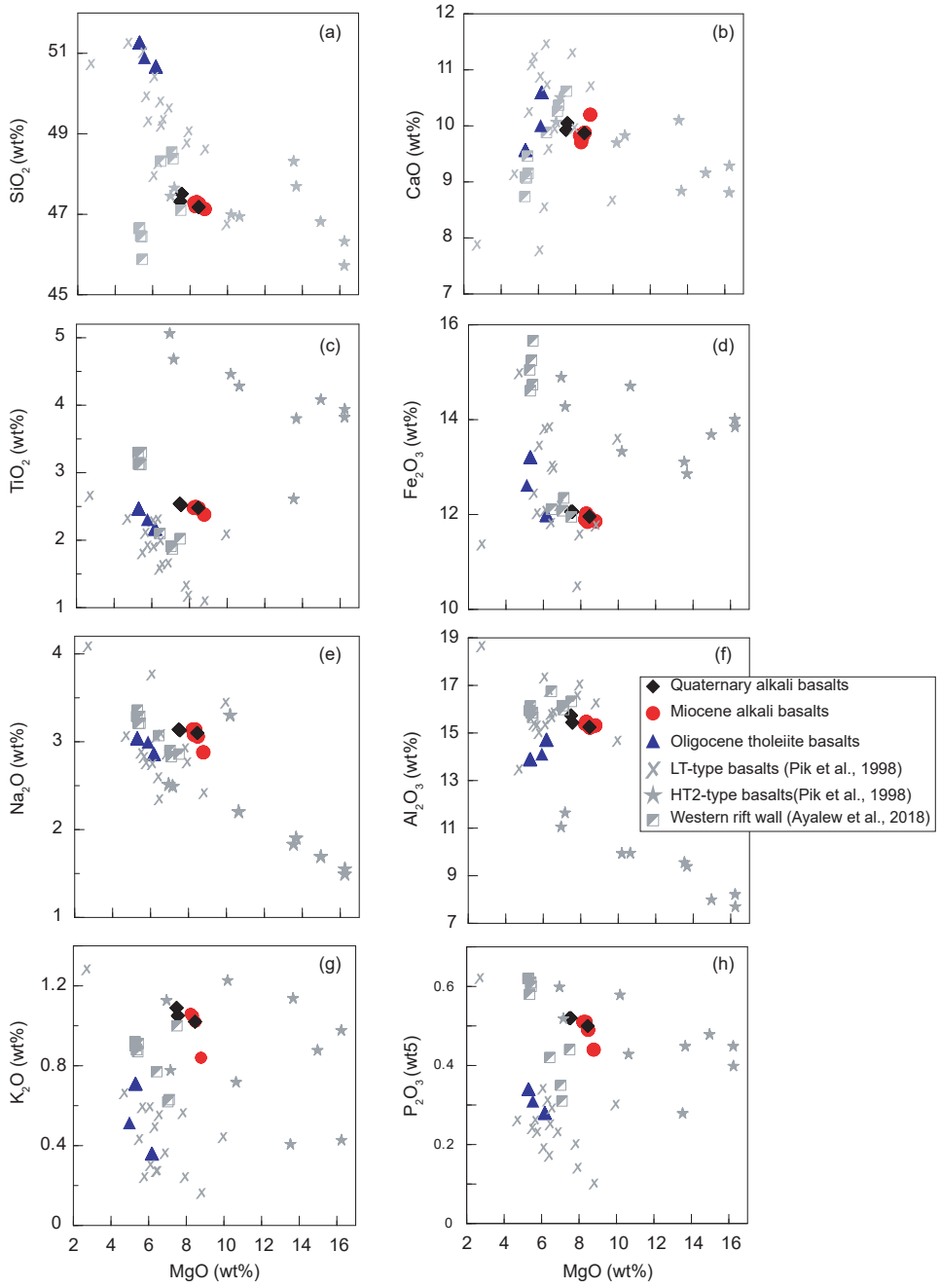

Figure 5. Variation diagrams of major element versus MgO for Kella basaltic rocks. LT- and HT2-type basalts are from Pik et al. (1998, 1999) and NMER western rift wall basalts are from Ayalew et al. (2018).

probably indicate the removal of olivine and clinopyroxene. However, thin section descriptions in these groups of basalts indicate minor plagioclase phenocrysts as compared with the dominant clinopyroxene and olivine phenocrysts; possibly indicating the start of plagioclase crystallizations were at later stage just as the magma ascending to the surface. and hence the plagioclase not fractionated from the melt.

The ratio CaO/Al_2O_3 decrease with a decrease in MgO for the Miocene and Quaternary alkaline basalts probably suggesting a fractionation of olivine and clinopyroxene. But the Oligocene tholeiitic basalts are defined by low MgO and high CaO/Al_2O_3, suggesting that olivine and plagioclase are the dominant fractionated phases. TiO_2 versus MgO also displays two negatively correlated fractionation trends (Figure 5c) where TiO_2 increase with decreasing MgO, indicating that there is no titanomagnetite fractionation for all groups of basalts. The petrographic descriptions indicate that opaque minerals are observed only as groundmass in all groups of basalts, which is also supporting the above inference of no titano-magnetite fractionation.

The concentrations of Ni and Cr of Miocene and Quaternary alkali basalts (Ni < 122 ppm and Cr < 460 ppm) and Oligocene tholeiite basalts (Cr < 100 ppm and Ni < 42 ppm) contents with low MgO values (5.28–6.11 wt. %) are lower than the ranges of primary magma [(Ni > 400–500 ppm), (Cr > 1000 ppm) and MgO (10–15 wt. %); Frey and Prinz, 1978] in equilibrium with a typical upper mantle mineral assemblage (Ayalew et al., 2016), showing that both alkali and tholeiitic basalts are highly fractionated. V is positively correlated with MgO in the Miocene and Quaternary alkaline and negatively correlated in the

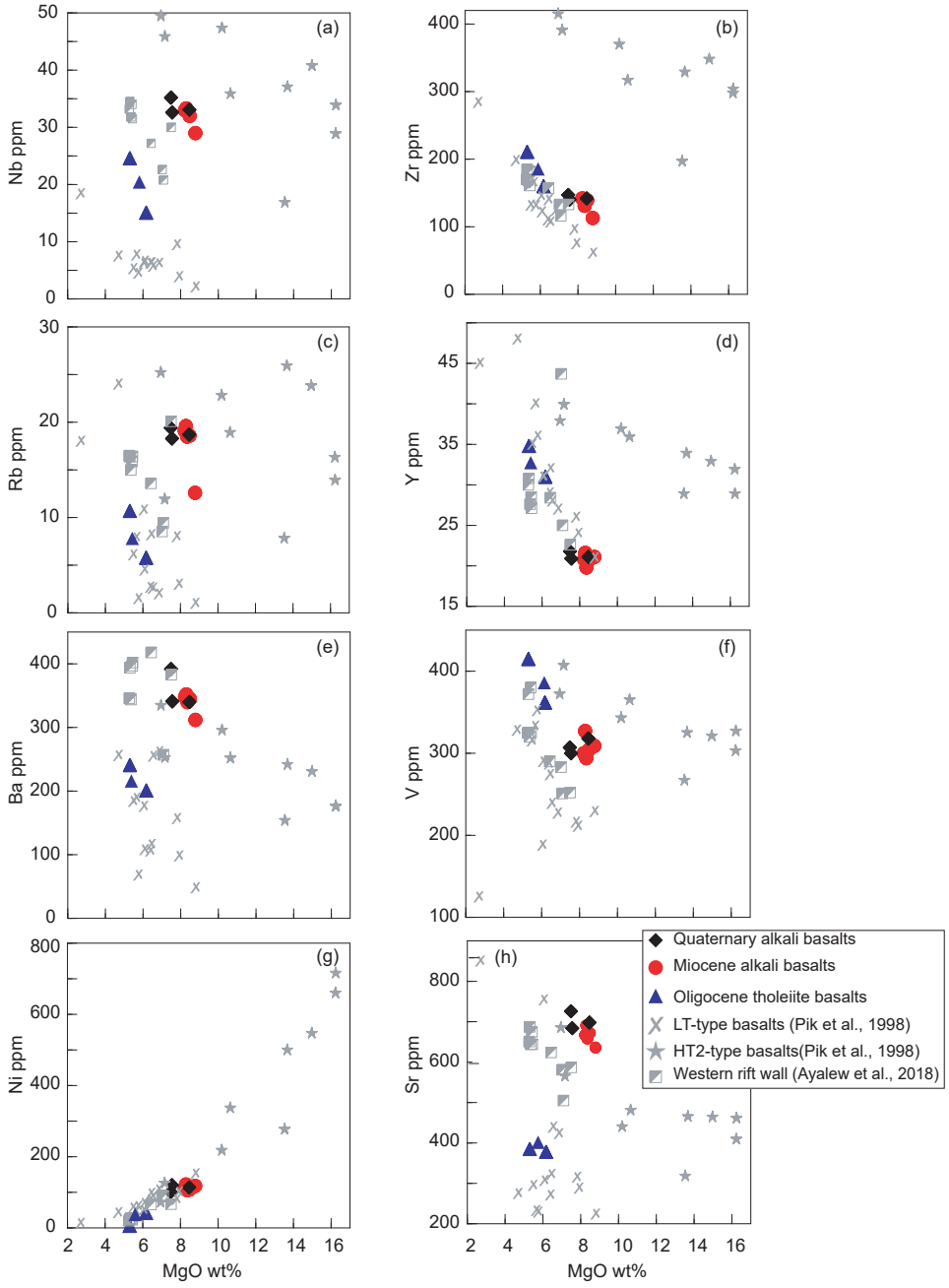

Figure 6. Variation diagrams of selected trace element versus MgO for Kella basaltic rocks. LT- and HT2-type basalts are from Pik et al. (1998, 1999) and NMER western rift wall basalts are from Ayalew et al. (2018).

Oligocene tholeiite lavas. These possibly indicate clinopyroxene fractionation in the Miocene and Quaternary alkali and the lack of clinopyroxene fractionation in the Oligocene tholeiite lavas.

Even though the basaltic groups cannot be co-magmatic because of their time gaps, there is a possibility of originating from similar mantle source that melted in different periods. However, the observed compositional variations between the Oligocene tholeiite group and the Miocene and Quaternary alkali groups by fractional crystallization cannot be the scenario to explain the compositional deviation among the groups. Therefore, these deviations clearly indicate that the Oligocene tholeiite group and the Miocene and Quaternary alkali groups have different petrogenesis and that fractional crystallization of a common source cannot explain these deviations.

6.2. *Effect of crustal contamination*

The Nb/U ratio of oceanic basalt has 47 ± 10 (Hofmann et al., 1986) and continental crust Nb/U ratios ~25 (Rudnick and Gao, 2004). Therefore, the Nb/U ratios of the Miocene and Quaternary alkali basalts (51.61–65.90) and the Oligocene tholeiite basalts (37.84–44.41) are within the range of mantle-derived oceanic basalts, implying that all groups of basalts in the study area were not crustally contaminated or with insignificant effect.

Ba/La, La/Nb, and Ba/Nb ratios are effective trace element ratios to asses potential contamination by crustal materials, where the values of crustal materials are Ba/La = 25, Ba/Nb = 54 and La/Nb = 2.2, and mantle-derived oceanic basalt ranges from Ba/La (4–16.6), Ba/Nb

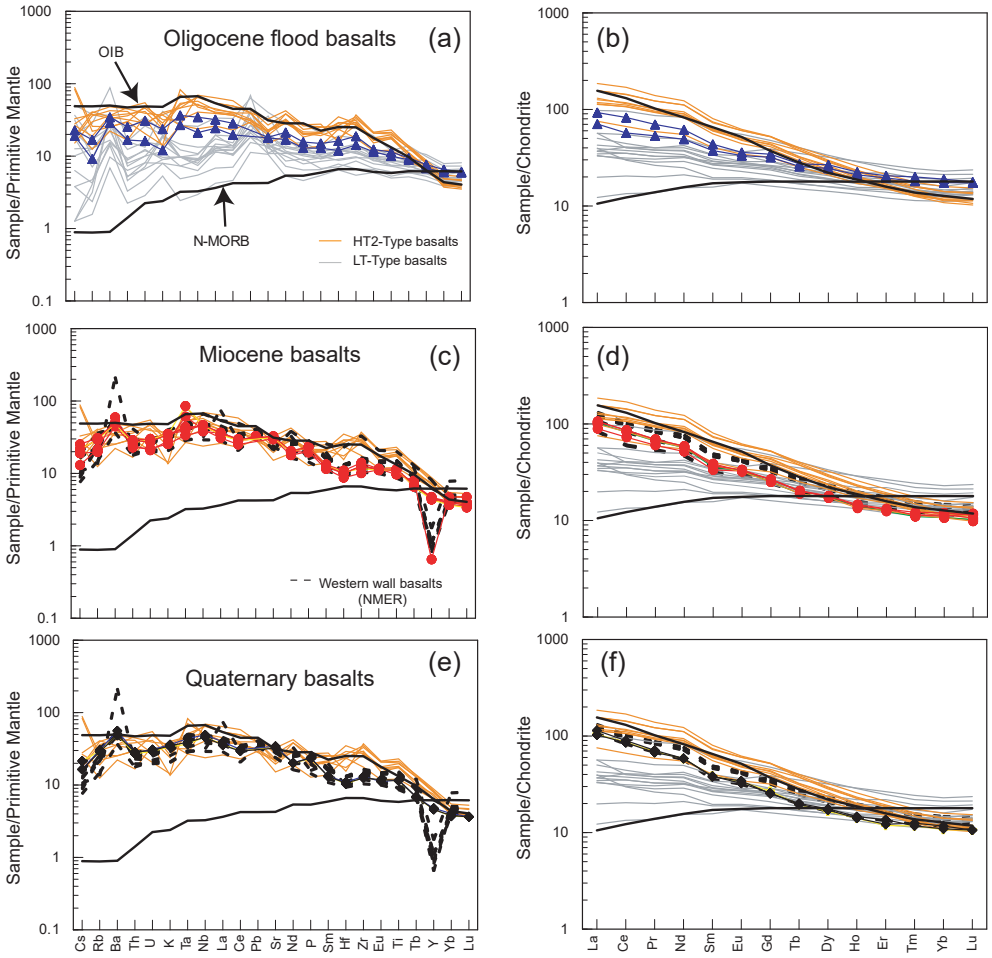

Figure 7. Primitive mantle-normalized multi-element and chondrite-normalized rare earth element (REE) patterns for representative samples from Kella basaltic rocks. Normalization values, typical oceanic island basalt (OIB) and Mid-Oceanic Ridge basalts (MORB) are from Sun and McDonough (1989). (a) for Oligocene basalts, (b) for Miocene basalts and (c) for Quaternary basalts. LT- and HT2-type basalts are from Pik et al. (1998, 1999) and NMER western rift wall basalts are from Ayalew et al. (2018).

(4.3–17.8), and La/Nb (0.66–1.32) (Weaver, 1991). Thus, even though variations are observed between the Oligocene tholeiite basalts (Ba/La = 10.95–12.03, Ba/Nb = 9.79–13.31 and La/Nb = 0.89–1.10) and the Miocene and Quaternary alkaline basaltic rocks (Ba/La = 13.76–14.71, Ba/Nb = 10.27–11.13 and La/Nb = 0.71–0.76) those ratios for all groups are within the range of typical mantle-derived values of Weaver (1991). Such characteristics trace element ratios may reflect insignificant crustal contamination in the genesis of all groups of basalts.

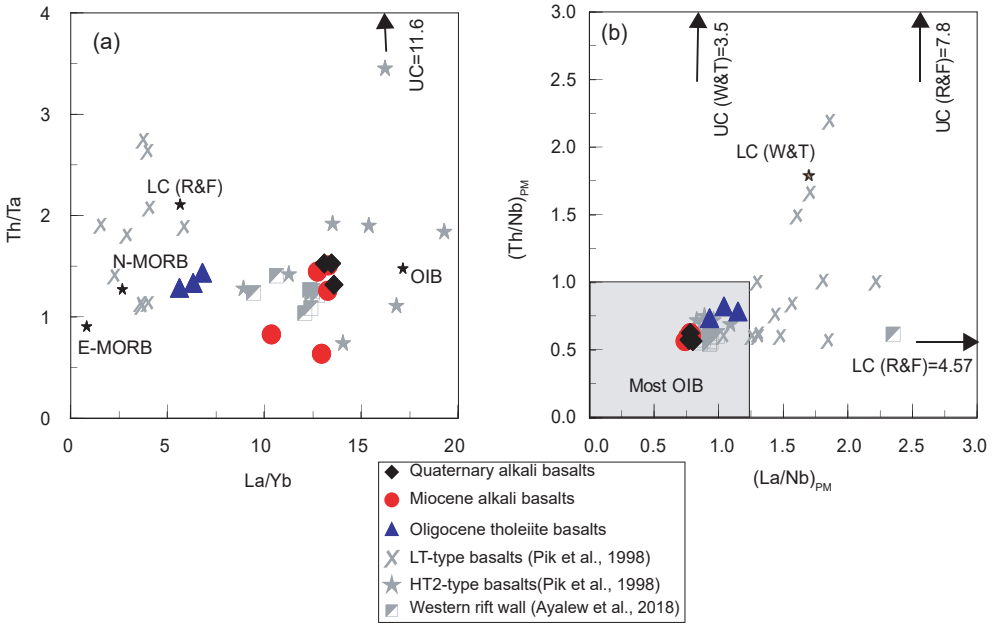

Figure 8. a) Th/Ta versus La/Yb and b) $(Th/Nb)_{PM}$ versus $(La/Nb)_{PM}$ variation of Kella basalts. Primitive mantle normalization values are from Sun and McDonough (1989). Composition of average upper (UC) and lower (LC) continental crust are from Rudnick and Fountain (1995) with Nb values from Weaver and Tarney (1984) and Barth et al. (2000). Labeled as (R&F) and (W&T), respectively. LT- and HT2-type basalts are from Pik et al. (1998, 1999) and NMER western rift wall basalts are from Ayalew et al. (2018). OIB, N-MORB and E-MORB field are from Sun and McDonough (1989), Pik et al. (1999) and Shinjo et al. (2011).

As shown in Th/Ta versus La/Yb (Figure 8a), all groups of basalts plotted within mantle values far from typical upper and lower continental crust value (Taylor and McLennan, 1981; Rudnick and Fountain, 1995). The tholeiitic basalts show more MORB affinities, whereas, the alkali basalts plotted towards the OIB value. $(La/Nb)_{PM}$ versus $(Th/Nb)_{PM}$ [subscript PM indicates ratios normalized to primitive mantle values of Sun and McDonough (1989)], relatively the Oligocene tholeiite basalts have higher $(Th/Nb)_{PM}$ and $(La/Nb)_{PM}$ than the alkali basalts (Figure 8b). But all the basalts from the study area plot within the field of uncontaminated oceanic island basalts (OIB) and do not follow trends toward typical upper continental crust nor lower crust (Weaver and Tarney, 1984; Rudnick and Fountain, 1995). Therefore, the incompatible trace element evidence indicates that upper and lower crustal contamination cannot be taken as the major controlling factor for the geochemical variations observed in both tholeiite and alkali basalts.

6.3. Partial melting and magma segregation depth

The temporal compositional deference among Oligocene tholeiite, Miocene and Quaternary alkali basalts are probably due to deferent depth of segregation and degree of melting. The Miocene and Quaternary Alkaline basalts have higher Gd/Yb ratios (2.71–2.97) and La/Yb ratios (10.39–13.62), whereas, the Oligocene tholeiite basalts have the lowest ratios of Gb/Yb (2.19–2.21) and La/Yb (5.64–6.83). As shown in Figure 9a, the Oligocene basalts are derived from shallow depth with higher degree of partial melting than the Miocene and Quaternary basalts.

The LREE/HREE and MREE/HREE variations are sensitive to the extent of melting and the amount of residual garnet in the source. Garnet strongly retains the HREE and therefore the presence of garnet in the source is the only phase that significantly fractionate the LREE/HREE [$(La/Yb)_N$ = 4.05–4.9 for the Oligocene tholeiite and 7.45–9.77 for the Miocene and Quaternary basalts] and MREE/HREE [$(Tb/Yb)_N$ = 1.44–1.47 for the Oligocene tholeiite and 1.67–1.81 for the Miocene and Quaternary basalts] ratios. Therefore, as shown in Figure 9b, the Miocene and Quaternary basalts are derived from mantle source with stability field of garnet-spinel transition zone at a depth of ~80 km (Takahashi and Kushiro, 1983), while the Oligocene basalts are from mantle source located within stability field of spinel facies more likely at shallower depth (<80 km) than the Miocene and Quaternary basalts.

In order to assess the melting conditions, we used non-modal equilibrium melting model of garnet- and spinel-bearing lherzolitic mantle source using primitive mantle (Sun and McDonough, 1989) as a staring source. Using La/Yb vs. Sm/Yb (Figure 10), the Miocene and Quaternary Alkali basalts can be produced with about 2% degree of partial melting close to spinel-garnet lherzolite transition zone mantle sources (50:50). Whereas the Oligocene Tholeiite basaltic group can be formed by equilibrium melting with 3–5 % degree of partial melting close to spinel lherzolite mantle source. Based on the model calculation the different ranges of MREE/HREE values among the Oligocene tholeiite and the Miocene and Quaternary alkali groups are explained by variable degree of melting and the amounts of residual garnet and spinel present in their mantle sources at different depths. Thus, the modeling result indicates that the Oligocene tholeiitic basaltic group and the Miocene-Quaternary Alkali basaltic groups originated from different depths. It is apparent from Figures 9 and 10, melting degree and the contribution of spinel lherzolite decreases from Oligocene to Quaternary time.

6.4. Mantle source variations

As shown in Figure 7, the Miocene and Quaternary basalts displayed REE patterns more similar to OIB–type. In these groups, the enrichment of light rare earth element (LREE) that suggests fractionation of light rare earth element (LREE) with respect to heavy rare earth (HREE) in the presence of garnet indicating that the sources for alkali basalts in the Miocene and Quaternary time may be located in the deep mantle sources.

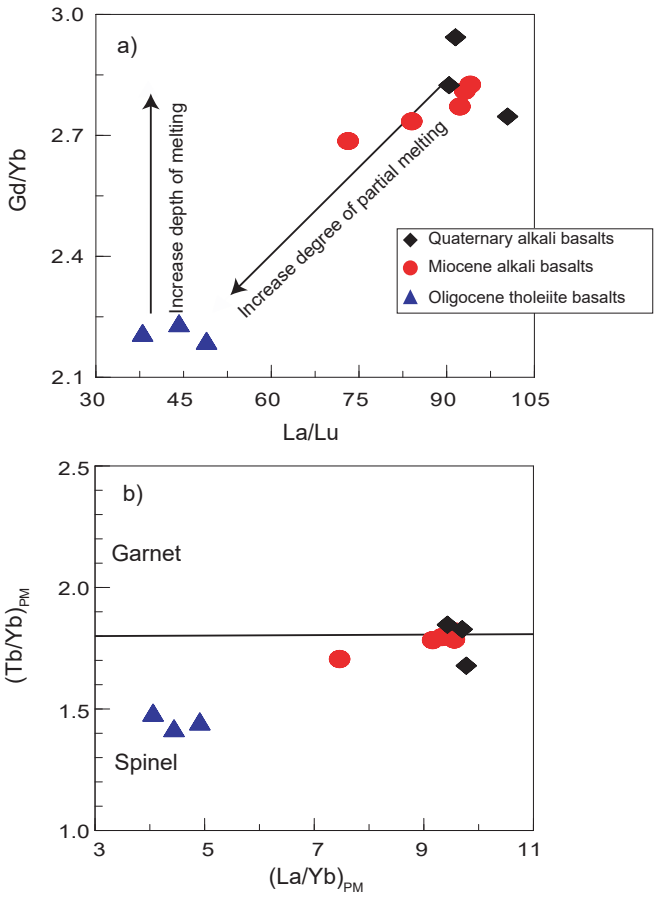

Figure 9. a) Gd/Yb versus La/Lu b) $(La/Yb)_{PM}$ versus $(Tb/Yb)_{PM}$ variations of Kella basalts. Primitive mantle normalization values are from Sun and McDonough (1989). Garnet/Spinel field is taken from Wang et al. (2002).

On the other hand, the Oligocene tholeiitic basalts are characterized by nearly horizontal slope from MREE to HREE, almost over-lapped the N-MORB pattern (Sun and McDonough, 1989). In terms of light rare earth elements, the Oligocene basalts show more enrichment than N-MORB. These characteristics may signify that the Oligocene basalts formed from garnet free shallow upper mantle source (Figure 9), probably an enriched or metasomatized asthenosphere mantle (E-MORB).

In the primitive mantle normalized patterns (Figure 7) the Miocene and Quaternary alkali basalts show more similarity to OIB-type pattern; however, the Oligocene tholeiitic basalts are relatively lower than the average OIB. Additionally, the Miocene and Quaternary alkali group have slight enrichment in HFSE (Nb and Ta) compared to the LILE (except Ba) and LREE (La and Ce) which is a typical characteristic feature in Oceanic Island basalts (OIB) patterns (Weaver, 1991). In contrast, the Oligocene tholeiitic basalts show no significant enrichment of HFSE (Nb and Ta) relative to LREE (La and Ce) and LILE, deviating from typical OIB-type mantle source (Sun and McDonough, 1989). In general, the Miocene and Quaternary Alkali basaltic groups are characterized by relatively higher HFSE/LREE and HFSE/LILE ratios compared with the Oligocene tholeiitic group, suggesting that their mantle source can be an OIB type (mantle plume).

As shown in Figure 11, Nb/Zr against Rb/Zr used to discriminate the mantle end-members involved in the genesis of all groups of basalts. Despite the difference in Rb/Zr and Nb/Zr ratios all groups of basalts are plotted within the mantle array. The Miocene and Quaternary alkaline basalts show an enrichment of Nb, Ba and Rb and most of the data are plotted near the OIB end-member. The Miocene and Quaternary alkaline basalts are characterized by higher Nb/Zr and Rb/Zr ratios. The alkaline basalts do not show any interaction with the crustal contaminants.

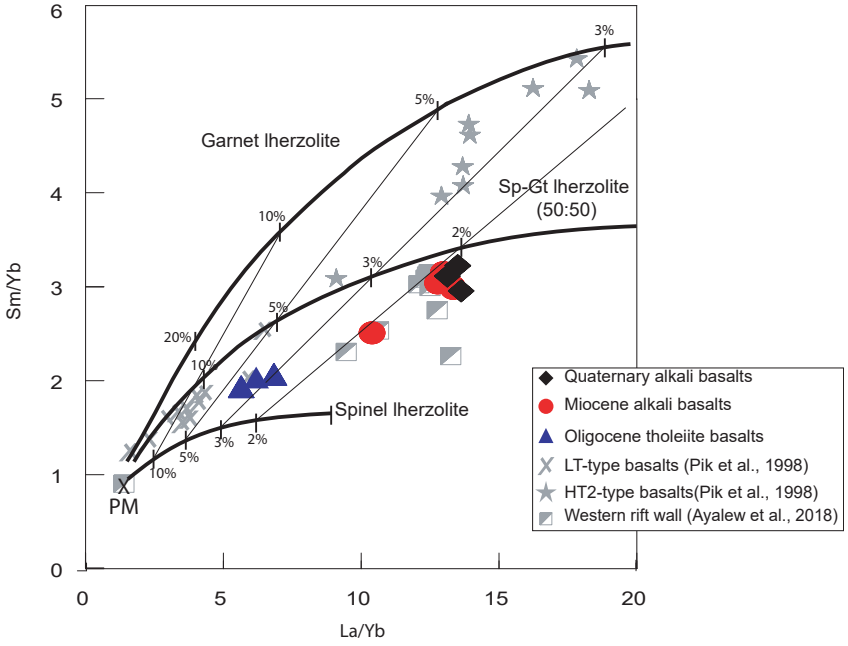

Figure 10. La/Yb versus Sm/Yb (B) variations of Kella basalts. Garnet and spinel lherzolites composition for modeling are modified from Aldanmaz et al. (2000), Zhao and Zhou (2007, 2009), Ayalew et al. (2018), Tamirat et al. (2021). PM from Sun and McDonough (1989).

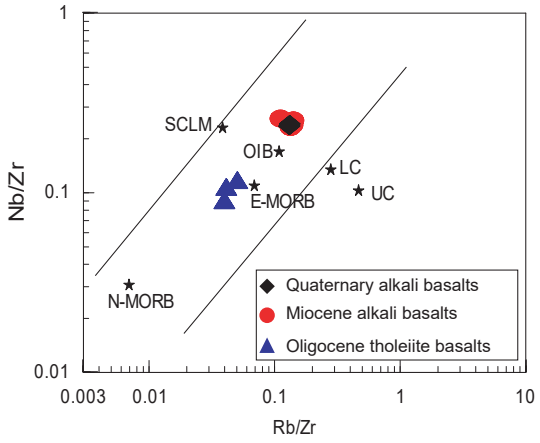

Figure 11. Rb/Zr versus Nb/Zr variations of Kella basalts. N-type MORB (N-MORB), E-type MORB (E-MORB), Oceanic Island basalt (OIB), and primitive mantle (PM) basalts values are from Sun and McDonough (1989). Upper (UC) and lower (LC) continental crust values are from Taylor and McLennan (1981). Subcontinental Lithospheric Mantle (SCLM) is from McDonough (1990).

Furthermore, in Nb/La versus Ti/Y diagram (Figure 12a) the Miocene and Quaternary alkaline basalts show higher Ti/Y and Nb/La ratios and fall close to OIB compositional range, indicating that their sources are associated with deep mantle source. In contrast, the Oligocene tholeiite basalts are relatively characterized by the depletion of Nb, Rb and Ba and have lower Nb/Zr and Rb/Zr ratios. The Oligocene tholeiite basalts are displaced from the E-MORB towards N-MORB end-member without any involvement of crustal contaminants (Figure 11). It is also displaying lower Nb/La ratios within the compositional range of E-MORB and N-MORB, suggest that the genesis of the basalts originated from asthenosphere derived magmas. As shown in Figure 12b, the Quaternary, the Miocene and the Oligocene basalts lie along a mixing line between OIB, E-MORB and N-MORB end-members.

As shown in Figures 11 and 12, at least three dominant mantle end-members are required to explain temporal source heterogeneity between the Miocene-Quaternary alkali basalts and the Oligocene tholeiitic basalts: (1) an OIB like component analogues to plume composition (Sun and McDonough, 1989), (2) an E-MORB like a component in the ambient asthenosphere), 3) a component similar to the N-MORB source (Sun and McDonough, 1989). The Miocene and Quaternary basalts are showing affinity from the average OIB towards E-MORB (Sun and McDonough, 1989), though dominantly with OIB-type component (Figure 12b). The linear trend along the average OIB and E-MORB in the Miocene and Quaternary basalts indicate a possible interaction of OIB-type plume with E-MORB component melt in their source origin.

With all the line of geochemical evidences, we envision a scenario that explains the genesis of basalts from the Oligocene, Miocene and Quaternary time magmatism in plateau-rift transition zone at central Main Ethiopian Rift. Magmatism in Ethiopia started with the arrival of a sub-lithospheric mantle plume (OIB; aka Afar Plume) which encountered a geochemically enriched mantle component (E-MORB) in the upper asthenosphere. The E-MORB could be that of an earlier depleted asthenospheric mantle wedge (N-MORB: minor relicts observed in Figures 7, 11, and 12) that later contaminated and enriched by subduction fluid/sediment during the Neoproterozoic subduction history of the area (Tamirat et al., 2021). Thus, the upwelling of the hot mantle plume (OIB) trigger melting of this E-MORB component in the upper asthenosphere and the plume (OIB) itself from garnet-spinel transition stability depth. The mixing between the dominant melts from E-MORB and minor melts from the plume (OIB) produce the Oligocene tholeiitic basalts of Ethiopian plateau at ~ 30 Ma (Pik et al., 1999). The progressive uprising of the mantle plume (OIB) generates more melts in itself due to more decompression. The mixing between dominant melts from the plume component (OIB) with minor E-MORB mantle component generates progressively both the Miocene and Quaternary alkali basalts [Miocene (10.6–8.3 Ma); Quaternary (<1.6 Ma)] (Abebe et al., 2010).

The results from this study show that metasomatized N-MORB (E-MORB) and mantle plume components have played a much more important role in the genesis of Oligocene, Miocene and Quaternary basaltic lavas. However, the previous studies in different part of Ethiopian magmatism suggested the contributions of lithosphere and upwelling depleted asthenosphere (Hart et al., 1989; Pik et al., 1998 and 1999; Furman, 2007), heterogeneous mantle upwelling (Kieffer et al., 2004) or interaction between an asthenosphere and an EM-like Pan-African continental lithosphere (Ayalew et al., 2018).

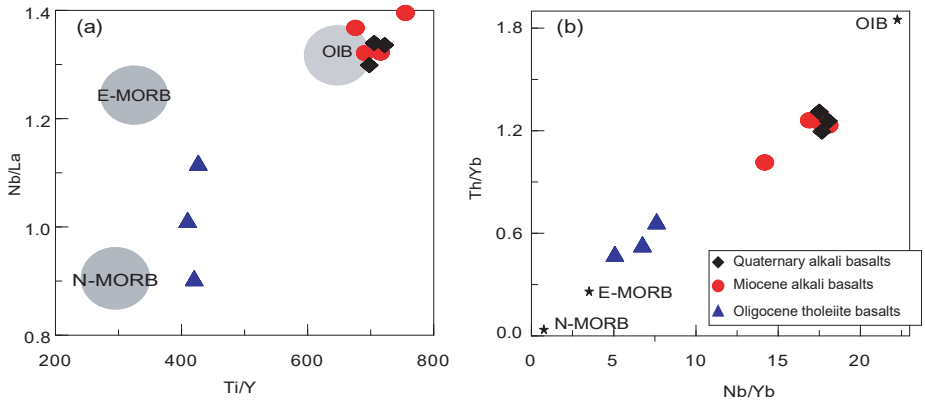

Figure 12. a) Nb/La versus Ti/Y b) Th/Yb versus Nb/Yb variations of Kella basalts. N-MORB, E-MORB and OIB (ocean island basalts) compositions are from Sun and McDonough (1989).

7. Conclusions

1. The Kella basaltic rocks consisting of the plateau (Oligocene flood basalt; 30-29 Ma), rift escarpment (Miocene basalt; 10.6–8.3 Ma) and rift floor (Quaternary basalt; <1.6 Ma) basalts.
2. The Oligocene basalts are holocrystalline and aphyric in texture with plagioclase and olivine micro phenocrysts <1 %. The Miocene basalts characterized by holocrystalline and moderately phyric texture with phenocrysts (clinopyroxene and olivine) up to 10%. The Quaternary basalts are holocrystalline and moderately phyric in texture with dominant phenocrysts (olivine and clinopyroxene) reach up to ~5%.
3. Major and trace element data of the Kella basaltic rocks exhibit two distinct groups; the Oligocene basalts are tholeiitic in composition while the Miocene and Quaternary basalts are alkaline in composition.
4. The geochemical variations among the groups reflect the involvement of two distinct mantle sources in their petrogenesis: i) the Oligocene tholeiite basaltic melts derived from enriched asthenosphere mantle source (E-MORB) and ii) the Miocene and Quaternary alkali basaltic melts show close similarity with ocean island basalts (OIBs) geochemistry, and this end member ascribed to the arrival of Afar plume head.
5. The geochemical modeling using garnet and spinel lherzolite reveals that the Oligocene tholeiite basaltic melts produced by equilibrium melting with 3–5 % degree of partial melting in spinel lherzolite mantle source, whereas the Miocene and Quaternary alkali basalts are produced with ~2% degree of partial melting within spinel-garnet lherzolite transition zone mantle sources.
6. Based on the geochemical evidences we suggested a scenario that explains the genesis of the Oligocene, Miocene and Quaternary basalts. The upwelling of the hot mantle plume (OIB) initiate melting of the E-MORB component in the upper asthenosphere and the plume (OIB) itself. The melted of the E-MORB component in the upper asthenosphere mixed with minor melts from the plume (OIB) produce the Ethiopian Oligocene tholeiitic flood basalts. The continues uprising of the mantle plume (OIB) generates more melts in the plume itself due to more decompression. The dominant melts from the plume (OIB) with minor E-MORB mantle component generates both Miocene and Quaternary alkali basalts.

Declarations

Author contribution statement

Daniel Meshesha, Takele Chekol & Sileshe Negussia: Conceived and designed the experiments; Performed the experiments; Analyzed and interpreted the data; Contributed reagents, materials, analysis tools or data; Wrote the paper.

Funding statement

This work was supported by Addis Ababa Science and Technology University (AASTU).

Data availability statement

Data included in article/supplementary material/referenced in article.

Declaration of interests statement

The authors declare no conflict of interest.

Additional information

No additional information is available for this paper.

Acknowledgements

We appreciate Central Laboratory of the Geological Survey of Ethiopia for thin section preparation and Australian Laboratory Services (ALS) for providing the major and trace element analyses result on time.

References

Abebe, T., Balestrieri, M.L., Bigazzi, G., 2010. The Central Main Ethiopian Rift is younger than 8 Ma: confirmation through apatite fission-track thermochronology. Terra. Nova 22 (6), 470–476.

Aldanmaz, E., Pearce, J.A., Thirlwall, M.F., Mitchell, J.G., 2000. Petrogenetic evolution of late Cenozoic, post collision volcanism in western Anatolia. Turkey: J. Volcanol. Geoth. Res. 102, 67–95.

Ayalew, D., 2000. Origin by fractional crystallization of transitional basalt for the Asela-Ziway pantellerites. Chem. Geol. 168, 1–3.

Ayalew, D., Barbey, P., Marty, B., Reisberg, L., Yirgu, G., Pik, R., 2002. Source, genesis and timing of giant ignimbrite deposits associated with Ethiopian continental flood basalts. Geochem. Cosmochim. Acta 66, 1429–1448.

Ayalew, D., Jung, S., Romer, R.L., Garbe-Schönberg, D., 2018. Trace element systematics and Nd, Sr and Pb isotopes of Pliocene flood basalt magmas (Ethiopian rift): a case for Afar plume-lithosphere interaction. Chem. Geol. 493, 172–188.

Ayalew, D., Jung, S., Romer, R.L., Kersten, F., Pfänder, J.A., Garbe-Schönberg, D., 2016. Petrogenesis and origin of modern Ethiopian rift basalts: constraints from isotope and trace element geochemistry. Lithos 1–14, 258–259.

Baker, J., MacPherson, C.G., Menzies, M.A., Thirlwall, M.F., Al-Kadasi, M., Mattey, D.P., 2000. Resolving crustal and mantle contributions to continental flood volcanism, Yemen; constraints from mineral oxygen isotope data. J. Petrol. 41, 1805–1820.

Barth, M.G., McDonough, W.F., L Rudnick, R., 2000. Tracking the budget of Nb and Ta in the continental crust. Chem. Geol. 165 (3-4), 197–213.

Beccaluva, L., Bianchini, G., Natali, C., Siena, F., 2009. Continental flood basalts and mantle plumes: a case study of the Northern Ethiopian plateau. J. Petrol. 50 (7), 1377–1403.

Beccaluva, L., Bianchini, G., Ellam, R.M., Natali, C., Santato, A., Siena, F., Stuart, M.F., 2011. Peridotite xenoliths from Ethiopia: inferences on mantle processes from plume to rift settings. Geol. Soc. Am. Spec. Pap. 478, 77–104.

Berhe, S.M., Desta, B., Nicoletti, M., Tefera, M., 1987. Geology, geochronology and geodynamic implications of the Cenozoic magmatic province in W and SE Ethiopia. J. Geol. Soc. (Lond.) 144, 213–226.
Bonini, M., Corti, G., Fabrizio, I., Manetti, P., Mazzarini, F., Abebe, T., Pecskay, Z., 2005. Evolution of the Main Ethiopian Rift in the frame of Afar and Kenya rifts propagation. Tectonics 24.
Chernet, T., Hart, W., Aronson, J., Walter, R., 1998. New age constraints on the timing of volcanism and tectonism in the northern Main Ethiopian Rift-southern Afar transition zone (Ethiopia). J. Volcanol. Geoth. Res. 80, 267–280.
Chorowicz, J., 2005. The East Africa Rift System. J. Afr. Earth Sci. 43, 379–410.
Corti, G., 2009. Continental rift evolution: from rift initiation to incipient break-up in the Main Ethiopian Rift, East Africa. Earth Sci. Rev. 96, 1–53.
Davidson, A., Rex, D., 1980. Age of volcanism and rifting in southwestern Ethiopia. Nature 283, 657–658.
Ebinger, C.J., Yemane, T., WoldeGebriel, G., Aronson, J.L., Walter, R.C., 1993. Late Eocene-recent volcanism and faulting in the southern main Ethiopian rift. J. Geol. Soc. London 150, 99–108.
Feyissa, D.H., Shinjo, R., Kitagawa, H., Meshesha, D., Nakamura, E., 2017. Petrologic and geochemical characterization of rift-related magmatism at the northernmost Main Ethiopian Rift: implications for plume-lithosphere interaction and the evolution of rift mantle sources. Lithos 282–283, 240–261.
Frey, F.A., Prinz, M., 1978. Ultramafic inclusions from San Carlos, Arizona: petrologic and geochemical data bearing on their petrogenesis. Earth Planet Sci. Lett. 38, 129–176.
Furman, T., 2007. Geochemistry of East African rift basalts: an overview. J. Afr. Earth Sci. 48, 147–160.
George, R., Rogers, N., Kelley, S., 1998. Earliest magmatism in Ethiopia: evidence for two mantle plumes in one flood basalt province. Geology 26, 923–926.
George, R., Rogers, N., 2002. Plume dynamics beneath the East African plate inferred from the geochemistry of the Tertiary basalts of southern Ethiopia. Contrib. Mineral. Petrol. 144, 286–304.
Girdler, R.W., 1983. Processes of rifting and break up of Africa. Tectonophysics 94, 241–252.
Hofmann, A.W., Jochum, K.P., Seufer, M., White, W.M., 1986. Nb and Pb in oceanic basalts: new constraints on mantle evolution. Earth Planet Sci. Lett. 79, 33–45.
Hofmann, C., Courtillot, V., Féraud, G., Rochette, P., Yirgu, G., Ketefo, E., Pik, R., 1997. Timing of the Ethiopian flood basalt event and implications for plume birth and global change. Nature 389, 838–841.
Hart, W.K., Woldegabriel, G., Walter, R.C., Mertzman, S.A., 1989. Basaltic volcanism in Ethiopia: constraints on continental rifting and mantle interactions. J. Geophys. Res. 94, 7731–7748.
Hayward, N., Ebinger, C., 1996. Variations in the along-axis segmentation of the Afar Rift system. Tectonics 15 (2), 244–257.
Irvine, T.N.J., Baragar, W.R.A.F., 1971. A guide to the chemical classification. J. Petrol. 54 (10), 2095–2123.
Kieffer, B., Arndt, N., Lapierre, H., Bastien, F., Bosch, B., Pecher, A., Yirgu, G., Ayalew, D., Weis, D., Jerram, D.A., Keller, F., Meugniot, C., 2004. Flood and shield basalts from Ethiopia: magmas from the African superswell. J. Petrol. 45, 793–834.
Le Bas, M.J., LeMaitre, R.W., Streckeisen, A., Zanettin, B., 1986. A chemical classification of volcanic rocks based on the total alkali-silica diagram. J. Petrol. 27 (3), 745–750.
Marty, B., Pik, R., Yirgu, G., 1996. Helium isotopic variations in Ethiopian plume lavas: nature of magmatic sources and limit on lower mantle contribution. Earth Planet Sci. Lett. 144, 223–237.
McDonough, W.F., 1990. Constraints on the composition of the continental lithospheric mantle. Earth Planet. Sci. Lett. 101, 1–18.
Meshesha, D., Shinjo, R., 2007. Crustal contamination and diversity of magma sources in the northwestern Ethiopia volcanic province. J. Mineral. Petrol. Sci. 102, 272–290.
Meshesha, D., Shinjo, R., 2008. Rethinking geochemical feature of the Afar and Kenya mantle plumes and geodynamic implications. J. Geophys. Res. 113, B09209.
Meshesha, D., Shinjo, R., 2010. Hafnium isotopic variations in Bure volcanic rocks fro northwestern Ethiopian Volcanic Province: a new insight for mantle source diversity. J. Mineral. Petrol. Sci. 105, 101–111.
Mohr, P., 1983. Ethiopian flood basalt province. Nature 303, 577–584.
Mohr, P., Zanettin, B., 1988. The Ethiopian flood basalt province. In: Macdougall, J.D. (Ed.), Continental Flood Basalts. Kluwer, Dordrecht, pp. 63–110.
Moore, J.M., Davidson, A., 1978. Rift structure in southern Ethiopia. Geology.
Natali, C., Beccaluva, L., Bianchini, G., Siena, F., 2016. Comparison among Ethiopia-Yemen, Deccan, and Karoo continental flood basalts of central Gondwana: insights on lithosphere versus asthenosphere contributions in compositionally zoned magmatic provinces. Spec. Pap. Geol. Soc. Am. 526, 191–215.
Peccerillo, A., Gezahegn, Y., Ayalew, D., 1995. Genesis of acid volcanics along the main Ethiopian rift: a case history of the Gedemsa volcano. SINET: Ethiop. J. Sci. 18, 23–50.
Pik, R., Deniel, C., Coulon, C., Yirgu, G., Hoffmann, C., Ayalew, D., 1998. The northwestern Ethiopian Plateau flood basalts: classification and spatial distribution of magma types. J. Volcanol. Geoth. Res. 81, 91–111.
Pik, R., Deniel, C., Coulon, C., Yirgu, G., Marty, B., 1999. Isotopic and trace element signatures of Ethiopian flood basalts: evidence for plume-lithosphere interactions. Geochem. Cosmochim. Acta 63, 2263–2279.
Ring, U., 2014. The East African Rift System. Aust. J. Earth Sci. 107/1, 132–146.
Rogers, N., Macdonald, R., Fitton, J.G., George, R., Smith, M., Barreiro, B., 2000. Two mantle plumes beneath the East African rift system: Sr, Nd and Pb isotope evidence from Kenya Rift basalts. Earth Planet Sci. Lett. 176, 387–400.
Rudnick, R.L., Gao, S., 2004. Composition of the continental crust. In: Holland, H.D., Turekian, K.K. (Eds.), Treatise on Geochemistry. 3. Elsevier, Amsterdam, pp. 1–64.
Rudnick, R.L., Fountain, D.M., 1995. Nature and composition of the continental crust: a lower crustal perspective. Rev. Geophys. 33, 267–309.
Saemundsson, K., 2010. East African Rift System-an overview. In: Geoscience of Rift Systems-Evolution of East Africa, pp. 1–18.
Scoon, R.N., 2018. Geology of National Parks of Central/Southern Kenya and Northern Tanzania. Springer International Publishing AG, part of Springer Nature, pp. 1–244.
Shinjo, R., Chekol, T., Meshesha, D., Taya, T., Tatsumi, Y., 2011. Geochemistry and geochronology of the mafic lavas from the southeastern Ethiopian rift (the East African Rift System): assessment of models on magma sources, plume-lithosphere interaction and plume evolution. Contrib. Mineral. Petrol. 162, 209–230.
Stewart, K., Rogers, N., 1996. Mantle plume and lithosphere contributions to basalts from southern Ethiopia. Earth Planet Sci. Lett. 139, 195–211.
Sun, S.S., McDonough, W.S., 1989. Chemical and isotopic systematics of oceanic basalts: implication for mantle composition and processes. Geol. Soc. Spec. Publ. 42, 313–345.
Takahashi, E., Kushiro, I., 1983. Melting of a dry peridotite at high pressures and basalt magma genesis. Am. Mineral. 68, 859–879.
Tamirat, T., Chekol, T., Meshesha, D., 2021. Petrology and geochemistry of basaltic rocks from north western Ethiopian plateau continental flood Basalt. J. Afr. Earth Sci. 182, 104282.
Taylor, S.R., McLennan, S.M., 1981. The composition and evolution of the continental crust: rare earth element evidence from sedimentary rocks. Phil. Trans. R. Soc. A301, 381–399.
Thompson, R.N., Morrison, M.A., Dickin, A.P., Hendry, C.L., 1983. Continental Flood Basalts Arachnids Rule, OK? Nantwich: Shiva, pp. 158–185.
Trua, T., Deniel, C., Mazzuoli, R., 1999. Crustal control in the genesis of Plio-Quaternary bimodal magmatism of the Main Ethiopian Rift (MER): geochemical and isotopic (Sr, Nd, Pb) evidence. Chem. Geol. 155, 201–231.
Ukstins, I.A., Renne, P.R., Wolfenden, E., Baker, J., Ayalew, D., Menzies, M., 2002. Matching conjugate volcanic rifted margins: 86 $^{40}Ar/^{39}Ar$ chrono-stratigraphy of pre- and syn-rift bimodal flood volcanism in Ethiopia and Yemen. Earth Planet Sci. Lett. 198 (3-4), 289–306.
Wang, K., Plank, T., Walker, J.D., Smith, E.I., 2002. A mantle melting profile across the Basin and Range, SW USA. J. Geophys. Res. 107 (b1), 2017.
Weaver, S.D., Tarney, J., 1984. Empirical approach to estimating the composition of continental crust. Nature 310, 575–577.
Weaver, B.L., 1991. The origin of ocean island basalt end-member compositions: trace element and isotopic constraints. Earth Planet Sci. Lett. 104 (2-4), 381–397.
WoldeGabriel, G., Aronson, J.L., Walter, R.C., 1990. Geology, geochronology, and rift basin development in the central sector of the Main Ethiopia Rift. Geol. Soc. Am. Bull. 102 (4), 439–458.
Wolfenden, E., Ebinger, C., Yirgu, G., Deino, A., Ayalew, D., 2004. Evolution of the northern Main Ethiopian rift: birth of a triple junction. Earth Planet Sci. Lett. 224, 213–228.
Zhao, J.H., Zhou, M.F., 2007. Geochemistry of Neoproterozoic mafic intrusions in the Panzhihua district (Sichuan Province, SW China): implications for subduction-related metasomatism in the upper mantle. Precambrian Res. 152, 27–47.
Zhao, J.H., Zhou, M.F., 2009. Secular evolution of the Neoproterozoic lithospheric mantle underneath the northern margin of the Yangtze Block, South China. Lithos 107, 152–168.